GPPF-2017-120

THE EFFECT OF THE TIME DELAY BETWEEN PRESSURE AND HEAT RELEASE RATE FOR LOW-ORDER MODELS OF THERMOACOUSTIC INSTABILITIES

Giulio Ghirardo
Ansaldo Energia Switzerland
Giulio.Ghirardo@ansaldoenergia.com
Baden, 5401, CH

Matthew P. Juniper
University of Cambridge
Dept. Engineering
mpj1001@cam.ac.uk
Cambridge, CB2 1PZ, UK

Mirko R. Bothien
Ansaldo Energia Switzerland
Mirko.Bothien@ansaldoenergia.com
Baden, 5401, CH

ABSTRACT

A successful low-order model introduced by Schuermans et al. [19], Noiray et al. [13] studies thermoacoustic instabilities assuming the fluctuating heat release rate q to be in phase with the acoustic pressure p, by neglecting the component of q out of phase with p. In this investigation we remove this hypothesis and consider a model in which, if p peaks at time t, q will peak at a later time $t + \tau$. We generalize the delay τ as the local slope of the flame phase response in the vicinity of the acoustic mode of interest with natural frequency ω_0. We present an alternative, simpler formulation of the problem and show that the low-order governing equations presented in [19,13] are actually the time derivative of it. We will first consider systems where two degenerate azimuthal modes oscillate, and then prove that most results apply also to systems where only one longitudinal mode oscillates.

In the linear regime, we show that the system has a higher linear growth rate than the model where the part of q not in-phase with p is neglected. This effect is larger for larger values of the product $\tau\omega_0$, with ω_0 being the natural frequency of oscillation of the acoustic system. We also discuss how the local slope of the flame phase response plays a role in (de) stabilizing the thermoacoustic system.

We then discuss in the nonlinear regime how to apply the method of averaging and the method of multiple timescales to this nonlinear problem, in particular accounting for the varying frequency of oscillation of the system, and validate the results with extensive numerical simulations. The resulting equations allow us to discuss the implications that a non-zero τ has on the capabilities of a successful

method of growth-rate extraction of Noiray and Schuermans [15]. We present mathematical evidence suggesting that, within the limits of certain approximations, the method should identify a good estimate of the growth rate despite the simplified assumptions, in line with the past experience of Bothien et al. [2].

See the end of the paper for a nomenclature.

1 INTRODUCTION

A successful state space low-order model for azimuthal thermoacoustic instabilities introduced by Schuermans et al. [19], and then further discussed by Noiray et al. [13], studies the dynamics of two dominant modes that behave like two oscillators coupled by the fluctuating heat release rate q. In this manuscript we neglect the effect of the transverse acoustic field on q, as studied previously by Ghirardo and Juniper [9] and assume that q depends only on the longitudinal acoustic field in the mean flow field direction. We also do not study the general case of a discrete number of flames, each modelled in terms of a generic flame describing function as carried out by Ghirardo et al. [10], and assume that the number of burners is large enough so that q can be approximated as homogeneous in the azimuthal direction, and the nonlinearity consists of a fundamental cubic saturation. We focus instead on the effect of the delay τ between pressure and heat release rate response, and more specifically on the local slope of the flame phase response in the vicinity of the acoustic frequency of the system. In particular, we want to answer the following questions:

- what is the effect on the frequency and the amplitude of oscillation, both in the linear and nonlinear regime?

- how do we apply successfully two vastly used nonlinear methods, accounting for the delay and the resulting change of the natural frequency of oscillation?

The answer to the first question will provide good practical insight into the role of the local slope of the flame response on the stability of the system. The answer to the second question and the resulting equations are crucial for the application of a whole body of work [12] and citations therein that aims to extract thermoacoustic linear growth rates, which in turn are often engineering design parameters in industry, e.g. for acoustic damper and liner design.

The manuscript is organised as follows. In §2 we briefly characterize the problem. In §3 we carry out the linear analysis, and discuss the boundary of stability of the system. In §4 we carry out the nonlinear analysis of the problem and discuss amplitudes and frequencies of the limit cycles. Both sections §3 and §4 are structured so that the mathematical discussion comes first, and the physical interpretation and results can be understood by a reader starting reading at §3.2 and §4.5 respectively. In §5 we discuss some implications of a non-zero for the growth rate extraction procedures.

2 BRIEF DERIVATION

Low-order models of azimuthal instabilities usually describe the system as a damped wave equation, with the fluctuating heat release rate q as a source term. The nondimensional equations are Noiray et al. [13], Ghirardo and Juniper [9]:

$$\frac{\partial u}{\partial t} + \frac{\partial p}{\partial \theta} = 0 \tag{1a}$$

$$\frac{\partial p}{\partial t} + \frac{\partial u}{\partial \theta} = q - \alpha p \tag{1b}$$

In (1) α is a positive damping coefficient, $p(t, \theta)$ is the fluctuating pressure, $u(t, \theta)$ is the fluctuating velocity in the azimuthal direction, with θ being the azimuthal angle in the periodic domain $[0, 2\pi)$. We focus on a rotationally symmetric system in the azimuthal direction θ, i.e. we assume that u, p, q do not have any direct dependence on θ. A discussion of the direct dependence on θ of the equation can be found in Noiray et al. [13]. A discussion of the effect of a discrete rotation group of symmetry, instead of full rotational symmetry, can be found in Ghirardo et al. [10].

We approximate the solution of (1) with a superposition of the two excited degenerate thermoacoustic modes, which at the flames positioned have shapes $\cos(n\theta)$ and $\sin(n\theta)$. As discussed in Ghirardo and Juniper [9] we can write:

$$\begin{cases} u(t,\theta) \approx n\eta_1(t)\sin(n\theta) - n\eta_2(t)\cos(n\theta) \\ p(t,\theta) \approx \eta_1'(t)\cos(n\theta) + \eta_2'(t)\sin(n\theta) \end{cases} \tag{2}$$

where here and in the following the prime denotes a time derivative, and n is the azimuthal wavenumber of the thermoacoustic mode we are studying. By substituting (2) into (1) and

by applying spatial averaging we obtain the equations:

$$\eta_1''(t) + \omega_0^2 \eta_1(t) = \langle q \rangle_{\cos}(t) - \alpha \eta_1'(t) \tag{3a}$$

$$\eta_2''(t) + \omega_0^2 \eta_2(t) = \langle q \rangle_{\sin}(t) - \alpha \eta_2'(t) \tag{3b}$$

where we introduce the spatial averaging operator for the generic function $m(\theta)$ as

$$\langle q \rangle_m(t) = \frac{1}{\pi} \int_0^{2\pi} q(\theta, t) m(\theta) d\theta \tag{4}$$

2.1 FLAME MODEL

We model the fluctuating heat release rate q as a nonlinear, time-invariant operator of the acoustic axial fluctuating velocity u_{ax} at the flame inlet. The reasoning behind this is that an acoustic fluctuation of the longitudinal velocity at the burner induces a perturbation of the fuel/air mixture fraction, and/or of the local flow field. This second perturbation is amplified by means of flow instabilities and/or modulates the swirl in swirling flames, and both mechanisms lead to perturbations of the flame response. For a review of these and other mechanisms, refer to Lieuwen [11], Ducruix et al. [5], Candel et al. [4]. The resulting transfer function typically involves a set of time delays τ_k, of standard deviations χ_k^2, and interaction indices n_k, all real valued quantities:

$$\frac{\hat{q}(\omega)}{\hat{u}_{\mathrm{ax}}(\omega)} = \sum_k \pm n_k e^{-i\omega\tau_k} e^{-\chi_k^2 \omega^2} \tag{5}$$

The fluctuating axial velocity u_{ax} can be expressed as a linear transfer function of the pressure p in the annular chamber, as long as only one mode, or two degenerate modes, oscillate, as discussed in detail in Ghirardo et al. [10]. In particular one can write

$$\frac{\hat{u}_{\mathrm{ax}}(\omega)}{\hat{p}(\omega)} = A^n(\omega) = \beta^*(\omega)e^{i\xi(\omega)} \tag{6}$$

where $A^n(\omega)$ is the admittance of the whole part of the combustor upstream of the section where u_{ax} is measured, calculated for the n-th azimuthal instability. From (5) and (6) it follows that

$$\frac{\hat{q}(\omega)}{\hat{p}(\omega)} = \beta^*(\omega)e^{i\xi(\omega)} \sum_{k=1}^{N_k} \pm n_k e^{-i\omega\tau_k} e^{-\chi_k^2 \omega^2} \tag{7}$$

Despite the quite complicated expression of (7), this transfer function typically exhibits a gain with a certain number of bumps[1] as function of the frequency, and a phase that decreases with frequency. This holds both in the linear and nonlinear regime, see e.g. Noiray et al. [14] for a matrix burner and Ghirardo et al. [8] for a swirl burner. This means that in the neighbourhood of the natural frequency ω_0 of the azimuthal mode of interest equation (7) can be simplified to:

$$\frac{\hat{q}(\omega)}{\hat{p}(\omega)} = \beta e^{-i(\psi + \tau\omega)} \qquad \text{for } \omega \text{ close to } \omega_0, \psi \in [-\pi, \pi) \tag{8}$$

---

[1] sequence of local maxima and minima alternating along the frequency axis

where τ is an equivalent time delay and describes the local slope of the phase response close to ω_0 and ψ is an offset of phase, and we choose a constant real valued gain β with frequency because in the general case there is no established trend, i.e. it can either grow or decay with frequency due to the bumps mentioned earlier. β is the linear gain of the flame response driving the oscillations. In the time domain, for $\psi = 0$ we can write that $q = \beta p(t - \tau)$, while for $\psi \neq 0$ one must formally introduce a linear time invariant operator $\mathcal{Q}$ such that $q = \mathcal{Q}[p(t - \tau)]$. In the following we simplify the discussion by setting $\psi = 0$, and generalize the results later. This allows us to interpret $\tau\omega$ as the phase between $\hat{q}$ and $\hat{p}$. In the time domain and in the nonlinear regime, we can write

$$q(t) = \beta p(t - \tau) - \kappa p(t - \tau)^3 \qquad (9)$$

In (9) we choose the nonlinear saturation first proposed by Noiray et al. [13], which is fundamental and simple, to focus on the effect of τ. In (9) κ is a positive value constant describing how fast with amplitude the flame response saturates. We refer the reader to Ghirardo et al. [10] to look at the effect of a generic nonlinear saturation of the flame on the spinning/standing nature and multistability of limit cycle solutions.

2.2 MODEL EQUATIONS

By substituting (9) into (3) we obtain

$$\eta_1''(t) + \omega_0^2 \eta_1(t) = f(\eta_1'(t), \eta_1'(t - \tau), \eta_2'(t - \tau)) \quad (10a)$$

$$\eta_2''(t) + \omega_0^2 \eta_2(t) = f(\eta_2'(t), \eta_2'(t - \tau), \eta_1'(t - \tau)) \quad (10b)$$

where $\omega_0 = n$ and the function f is defined as:

$$f(a, a_\tau, b_\tau) \equiv a_\tau \left[\beta - \frac{3}{4}\kappa \left(a_\tau^2 + b_\tau^2 \right) \right] - \alpha a \qquad (11)$$

where we denote with a subscript τ a delayed quantity, e.g. $a_\tau(t) = a(t - \tau)$. An example of a time domain simulation of the oscillators (10) is presented in Fig. 1, where in a) the continuous thin lines are the fast oscillating signals $\eta_1(t)$ and $\eta_2(t)$, and the thick lines are their slowly varying amplitudes of oscillation $A_1(t)$ and $A_2(t)$. In Fig. 1.b we present the instantaneous frequency of oscillation of the same simulation with a black line. To link this study with the existing literature, we remark that one can take the time derivative of (10) and obtain:

$$\zeta_1''(t) + \omega_0^2 \zeta_1(t) = \frac{\partial}{\partial t} f(\zeta_1(t), \zeta_1(t - \tau), \zeta_2(t - \tau)) \quad (12a)$$

$$\zeta_2''(t) + \omega_0^2 \zeta_2(t) = \frac{\partial}{\partial t} f(\zeta_2(t), \zeta_2(t - \tau), \zeta_1(t - \tau)) \quad (12b)$$

where the function $\zeta_j(t) \equiv \eta_j'(t)$ was introduced. By setting τ to zero in (12) one recovers the equations discussed in Noiray et al. [13]. One disadvantage of the second formulation (12) of the problem is the additional time-derivative of the function f that includes the heat release rate and leads to the study of the problem with mixed terms $\zeta_j^k(t)\zeta_j'(t)$ in the equations.

We mention that any stochastic contribution $q_s(t)$ to the heat release rate appears on the right hand sides of (10) after spatial averaging, and hence should appear in (12) as time derivative, and not outside of the time derivative as presented in Bonciolini et al. [1]. We stick to the formulation in terms of equations (10) in the following.

2.3 RANGE OF THE PARAMETERS $\{\alpha, \beta, \tau\omega_0\}$

In this manuscript all the analytical expressions are valid for $\{\beta, \alpha, \tau\} \in \mathcal{R}^{+3}$ unless otherwise indicated. It is however important to estimate the range of typical values of these parameters in thermoacoustics. We will present graphically the results only for this range of values, with the exception of Figures 2, 3.a and 3.b. We now proceed in estimating ranges for the damping and driving coefficients α, β and of τ.

We consider a reasonable thermoacoustic instability with a ratio σ/ω_0 of the growth rate to the natural frequency of oscillation of 0.05. We also assume that the system without a flame has an overall level of acoustic damping such that the growth rate of the system when the flame's response is artificially shut off is -0.04[2]. We then consider the case of a zero time delay τ, for which the growth rate of the system is $(\beta - \alpha)/2$ as discussed in [13]. The two assumptions lead to the value of $\alpha/\omega_0 = 0.08$ and $\beta/\omega_0 = 0.18$, and a ratio $\beta/\alpha = 2.25$, in line with values reported in Noiray et al. [13], Bothien et al. [2]. Accounting for more unstable flames, we then decide to study in the following the system for $\beta/\alpha \in [0, 3]$ as a relevant range for thermoacoustic instabilities, while we will keep constant the value of $\alpha/\omega_0 = 0.08$ as just calculated. We fix α to this value because the plots are more sensitive to β/α and $\tau\omega_0$ than to the value of α, and varying all three parameters at the same time would require three dimensions. We will reconsider the effects of the absolute value of α at the end of §3.2.

For estimating the range for $\tau\omega_0$, we consider an example of a thermoacoustic mode at $f = 300\,\mathrm{Hz}$, subject to a convective time delay of $\tau = 5\,\mathrm{ms}$. This leads to a product of $\tau\omega_0 \approx 3\pi$. Notice moreover that the superposition of different time delays often leads to a steeper phase response in certain frequency ranges. In these ranges, the equivalent time delay $\tau\omega_0$ discussed just after (8) would be even larger. Accounting for longer time delays and larger frequencies of oscillation, in the following we study the system for $\tau\omega_0 \in [0, 8\pi]$.

3 LINEAR ANALYSIS

In this section we study the boundary of linear stability of (10). We proceed by retaining only the linear terms in (10a) and (10b), and obtain:

$$\eta_j''(t) + \alpha\eta_j'(t) - \beta\eta_j'(t - \tau) + \omega_0^2\eta_j(t) = 0 \qquad j = 1, 2 \quad (13)$$

We substitute $\eta_1(t) = e^{(\sigma + i\omega)t}$ into (13) where σ is the growth rate and ω the real valued angular frequency of oscillation, and obtain the characteristic equation. We then split the equation

---

[2]the modelling carried out in Ghirardo et al. [10] of an annular combustor led to a $\sigma/\omega = -0.05$ for the first azimuthal mode when the flame was off i.e. $\beta, \kappa = 0$
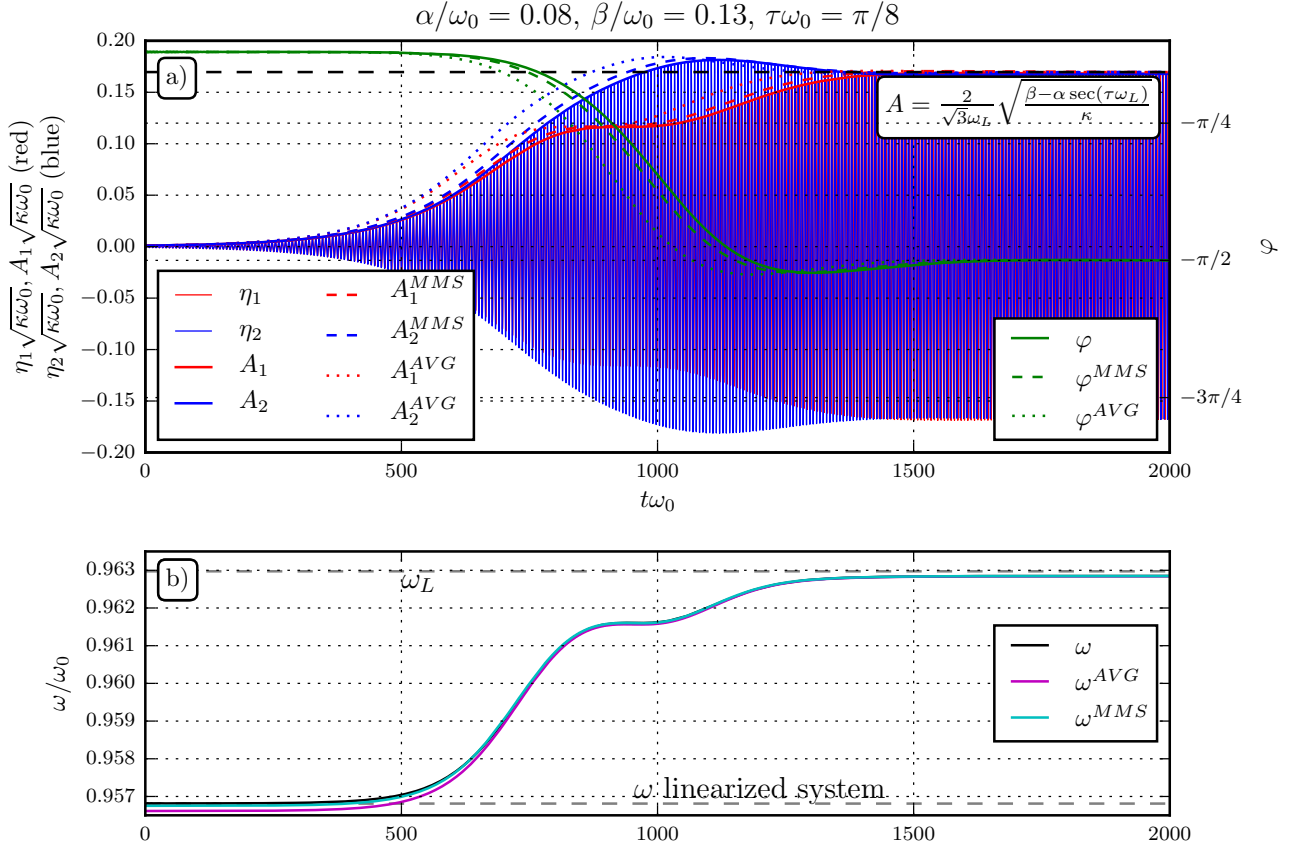
Figure 1: a) Example of time domain simulation in terms of the original system of equations (continuous lines), after applying the method of multiple scales (MMS, dashed lines) and after applying the averaging method (AVG, dotted lines). In this case we choose $\tau\omega_0 = \pi/8 \neq 0$ and this leads to a non-trivial response: the two amplitudes A_j undergo a non-monotonic transient where A_1 overshoots the final amplitude and A_2 grows more slowly than A_1; b) Dependence of the frequency of oscillation on time: ω is the calculated instantaneous frequency of oscillation extracted from the time series η_j, while ω^{AVG} and ω^{MMS} are the predicted instantaneous frequencies using the method of multiple scales (MMS) and the averaging method (AVG)

into real and imaginary parts and after some manipulation obtain:

$$\frac{\beta\cos(\tau\omega)e^{-\sigma\tau} - \alpha}{2} = \sigma\left[1 + \frac{\beta\tau}{2}\mathrm{sinc}(\tau\omega)e^{-\sigma\tau}\right] \quad (14a)$$

$$\omega^2 - \omega_0^2 + \beta\omega\sin(\tau\omega)e^{-\sigma\tau} = \sigma^2 + \alpha\sigma - \beta\sigma\cos(\tau\omega)e^{-\sigma\tau} \quad (14b)$$

We study for which parameters $\{\alpha, \beta, \tau\} \in \mathbb{R}^{+3}$ the system is neutrally stable, i.e. there exist real-valued solutions ω_L of the system of equations (14) when setting the growth rate σ to zero:

$$\beta\cos(\tau\omega_L) - \alpha = 0 \quad (15a)$$

$$\omega_L^2 - \omega_0^2 + \beta\omega_L\sin(\tau\omega_L) = 0 \quad (15b)$$

We carry out with rigour the analysis of the implicit dispersion relation $\omega_L = \omega_L(\beta/\alpha, \tau\omega_0)$ in the following section §3.1. The impatient reader will find the results of the linear stability analysis presented in §3.2.

3.1 DETAILED DERIVATION

By studying as a function of σ the left and right hand sides of (14a), we find that there exists only one solution for the growth rate σ, and that it is positive if $\beta\cos(\tau\omega) - \alpha > 0$. It follows that equation (15a) defines the boundary of stability, with the system being unstable if the left hand side is positive. We also observe from (15b) that when on the boundary, if τ is zero, ω_L matches the natural frequency of oscillation ω_0. We observe that if (α, β, τ) provide a real-valued solution ω_L of (15), then (α, β, τ_k) is a solution too, with

$$\tau_k = \tau + 2k\pi/\omega_L, \qquad k \in \mathbb{N}^+. \quad (16)$$

We can then initially limit the search of solutions restricting the domain of τ to

$$\tau \in \left[-\frac{\pi}{\omega_L}, \frac{\pi}{\omega_L}\right) \quad (17)$$

and then exploit (16) to generate the other solutions. Since ω_L is close to the natural frequency of the system, ω_0, the domain (17) is bounded. Moreover, since α and β are positive, equation (15a) allows us to further restrict the domain so that the cosine term is positive:

$$\tau \in \left[-\frac{\pi}{2\omega_L}, \frac{\pi}{2\omega_L}\right) \quad (18)$$

4

This is in line with the Rayleigh criterion [16]: the phase difference between q and p must be in the range $(-\pi/2, \pi/2)$ to cause instability.

The domain (18) allows negative values of τ, though a negative value in the system does not make physical sense. We investigate negative solutions nonetheless, because they lead to positive solutions τ_k by the application of (16). The neutrality of the solutions is defined by (15a), from which we can calculate the reduced linear driving β_L at the onset of instability as a function of α and τ:

$$\beta_L = \alpha \sec(\tau \omega_L), \tag{19}$$

The frequencies of the neutrally stable solutions are the solutions ω_L of (15b). We substitute β from (19) into (15b) and obtain:

$$h(\tau, \omega_L) \equiv \omega_L^2 - \omega_0^2 + \alpha \omega_L \tan(\tau \omega_L) = 0 \tag{20}$$

Since we cannot solve ω_L as a function of τ from (20) analytically, we present in Fig. 2 a contour plot of h/ω_0^2, in the restricted domain (18). The solution of (20) is the implicit curve satisfying $h/\omega_0^2 = 0$, reported with the black line. There are two solutions ω_L for each value of τ if $\hat{\tau} < \tau < 0$, with $\hat{\tau}\omega_0 \approx -1.13$. This black line shows the effect of $\tau\omega_0$ on the frequency shift, ω_L/ω_0, on the border of neutral stability. We present in Fig. 3.a the same curve $h = 0$, but colour
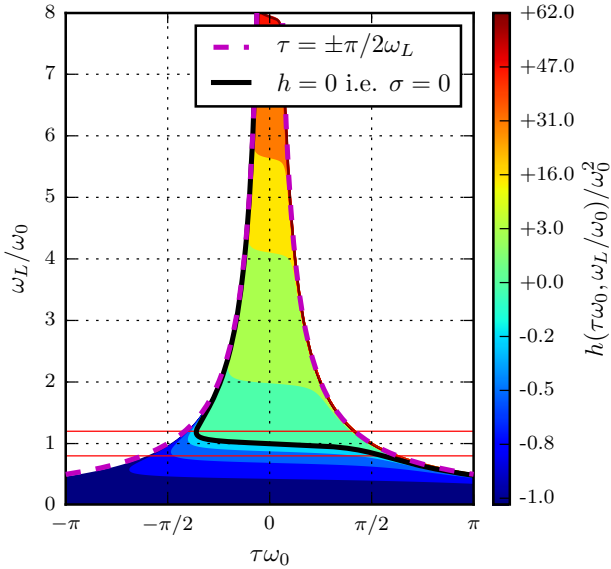

Figure 2: Contour plots of h from equation (20). On the black line $h = 0$, i.e. equation (15) is satisfied and the system is neutrally stable. The two horizontal red lines ($\pm 20\%$ in frequency) highlight the approximate range for thermoacoustic applications

it based on the value of the ratio β/α that makes the system neutrally stable and zoom to the range of parameters typical of thermoacoustic applications discussed in §2.3. We present in Fig. 3.b the same information but invert the vertical axis and the colourmap. We then recover the full boundary of neutral stability by applying the transformation (16) to values of

$(\beta/\alpha, \tau\omega_0)$ from Fig. 3 and present it in Fig. 4. For comparison with the previous work of Schuermans et al. [19], Noiray et al. [13], we now make the same assumption and set to zero the part of the heat release rate q out of phase with p. The $\sin(.)$ term in equations (15b) disappears, and the equations (15) simplify to

$$\beta \cos(\tau \omega_L) - \alpha = 0 \tag{21a}$$
$$\omega_L^2 - \omega_0^2 = 0 \tag{21b}$$

In equations (21) we find that regardless of the values of α, β and τ the linear frequency of oscillation at the neutral boundary of stability coincides with the natural acoustic frequency of the unperturbed oscillator:

$$\begin{cases} \beta &= \alpha/\cos(\tau \omega_0) \\ \omega_L &= \omega_0 \end{cases} \tag{22}$$

These results are presented in Fig. 3 and 4 with black lines.

Generalization for $\psi \neq 0$ One looks for the solution of (15) where the additional term $-\psi$ appears in the equations:

$$\beta \cos(\tau \omega_L - \psi) - \alpha = 0 \tag{23a}$$
$$\omega_L^2 - \omega_0^2 + \beta \omega_L \sin(\tau \omega_L - \psi) = 0 \tag{23b}$$

One can generate a solution for (23) from the solution of (15). In particular, we observe that if $\{\alpha, \beta, \tau^{\psi=0}\omega_0\}$ lead to a neutrally stable frequency ω_L/ω_0 in (15), then $\{\alpha, \beta, \tau^\psi\omega_0\}$ lead to the same frequency ω_L/ω_0, with $\tau^\psi\omega_0$ calculated as:

$$\tau^\psi \omega_0 = \tau^{\psi=0}\omega_0 + \frac{\psi}{\omega_L/\omega_0} \tag{24}$$

This leads to a constant shift of the minima of the troughs of Fig. 4.a and of the zeros of 4.b, originally at multiples of 2π for $\psi = 0$, to ψ plus multiples of 2π, since the term ω_L/ω_0 in (24) is one at the minima. Moreover on each of the troughs, we find from (24) that points at larger $\tau\omega_0$ than the minimum are shifted to values larger than ψ because $\omega_L/\omega_0 < 1$ there, and points at smaller $\tau\omega_0$ than the minimum are shifted to values smaller than ψ because $\omega_L/\omega_0 > 1$. The solutions for a few selected values of ψ is reported in Fig. 5, where the shift of $+\psi$ is clearly visible, while the additional shift just mentioned is not visible with the naked eye.

3.2 DISCUSSION

We present in Fig. 4.a the stability map of the system, where the ranges of the horizontal and vertical axes are representative of a class of thermoacoustic systems as discussed in §2.3. The ratio β/α, where β is the linear driving coefficient of the flame response and α the acoustic damping coefficient, is reported with a coloured line as a function of the equivalent delay $\tau\omega_0$ introduced in (8), where ω_0 is the natural acoustic frequency of the system and τ is the slope of the flame phase response close to ω_0. Above this boundary of stability the system is linearly unstable and the region is coloured with grey. The colour of the boundary is the linear frequency of oscillation
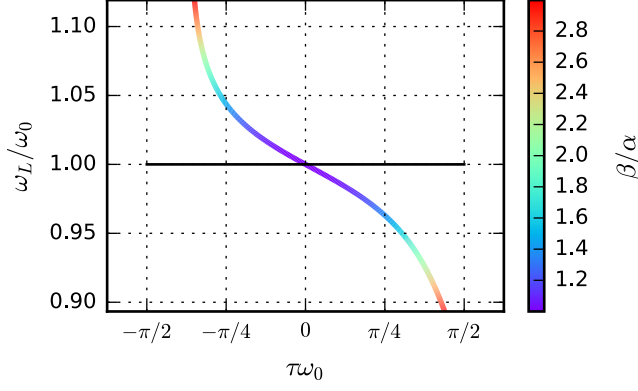
(a) frequency of neutral stability
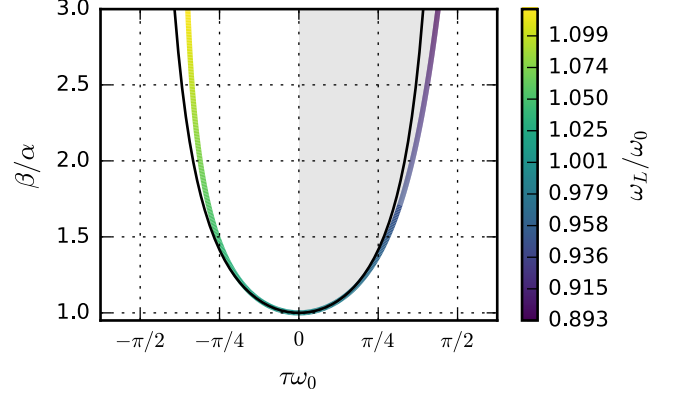
(b) ratio β/α of driving over damping at neutral stability

Figure 3: a) The coloured line is the frequency of the neutrally stable modes as a function of $\tau\omega_0$. This is the black line presented first in Fig. 2, coloured with the values of β/α that make the system stable. b) stability map of the system. This is the same data of a) but swapping the vertical axis with the colormap. The coloured line represents the values of β/α as a function of τ on which the system is neutrally stable. We study the system for positive values of $\tau\omega_0$, where the linearly unstable region is reported in gray. The same analysis on the system obtained by neglecting the component of q not in phase with p as done in Schuermans et al. [19], Noiray et al. [13] is reported with black lines in frames a) and b)

ω_L/ω_0 of the system and the respective colormap is reported on the right.

Where $\tau\omega_0$ is a multiple of 2π we have that $\omega = \omega_0$ and q is exactly in phase with p, and the required ratio β/α to make the system neutrally stable equals unity and is minimum, as expected from the Rayleigh criterion. As the value of $\tau\omega_0$ gets further from a multiple of 2π, the strength of the flame response required to de-stabilize the system increases, and the curve β/α takes the form of a trough with the minimum at each multiple of 2π.

Moreover, the width of the troughs increases along the increasing multiples of 2π, so that the boundary of stability approaches the horizontal asymptote $\beta/\alpha = 1$ as $\tau\omega_0 \to \infty$. This means that for a given system with a fixed ratio of β/α, flames governed by large time delays, i.e. equivalently flames with a steep phase response in the vicinity of the acoustic frequency ω_0, are more likely to be unstable than flames governed by smaller time delays, and the overall system stability is less affected by the phase response of the flame close to the frequency of oscillation. In other words, for a fixed flame gain, a flame with a steeper phase response is more likely to trigger an acoustic mode, because the troughs in Fig. 4.a are wider. This can be intuitively be understood by the fact that, if the flame has a steep phase response at the resonance frequency ω_0, even a little shift of the frequency from ω_0 leads to strong variations of the phase between q and p.

We present the frequency of oscillation ω_L also in Fig. 4.b. Where $\tau\omega_0$ is a multiple of 2π the frequency ω_L matches the natural frequency of oscillation ω_0. For values of the time delay $\tau\omega_0 < \pi/2$ the linear frequency of oscillation ω_L is smaller than the natural frequency of oscillation ω_0. We observe that for values of $\beta/\alpha < 3$ we can see a linear frequency shift of about 10%[3] even for small values of $\tau\omega_0$, and that this

shift is larger at large values of $\tau\omega_0$ because the branches are less steep for large $\tau\omega_0$. This will be confirmed in §4 also in the nonlinear regime, and shows how assuming that the frequency of oscillation of the system matches the natural frequency of oscillation ω_0 is a rough approximation.

We now consider what happens when $\tau\omega_0$ is π plus a multiple of 2π, and consider for example the case of $\tau\omega_0 = 7\pi$. We observe that the phase difference between q and p at ω_0 is $\pm\pi$, hence the Rayleigh criterion at the natural acoustic frequency ω_0 is negative and the system cannot oscillate at ω_0. One is then tempted to conclude that the acoustic mode at ω_0 will be stable and pulsations will not be observed. What actually happens is that for values of $\beta/\alpha \gtrsim 2.5$ the part of q not in phase with the pressure p is strong enough to lead to a frequency shift $|\omega_L - \omega_0|$ large enough so that the absolute value of the phase difference between q and p at ω_L is smaller than $\pi/2$ and then leads to a positive Rayleigh contribution, destabilizing the system. This happens in this case on two branches, which in Fig. 4.a intersect at $(\tau\omega_0, \beta/\alpha) \approx (7\pi, 2.5)$, and in Fig. 4.b belong to frequencies smaller and larger than ω_0 at $\tau\omega_0 = 7\pi$. When more than one branch is possible, numerical evidence suggests that the system converges to the one with higher growth rate. This least favourable case of $\tau\omega_0$ being π plus a multiple of 2π should have clarified the common misconception that an acoustic mode at ω_0 will not pulsate if the phase difference between flame response and pressure at ω_0 is not favourable. Indeed, it is quite likely that β/α will be large enough and/or the local phase slope $\tau\omega_0$ will be steep enough to make the same acoustic mode at ω_0 pulsate at a frequency ω_L where it is unstable.

This analysis shows that given a combustor with a fixed random but physical set of acoustic modes $\{\omega_0^k, k = 1, 2\ldots\}$, flames governed by large values of τ, e.g. characterized by long time delays, are situated to the right of Fig. 4 where the boundary of stability is closer to the line β/α, and: *i)* are

[3]in line with experiments, see Boudy et al. [3] for evidence for an academic test rig
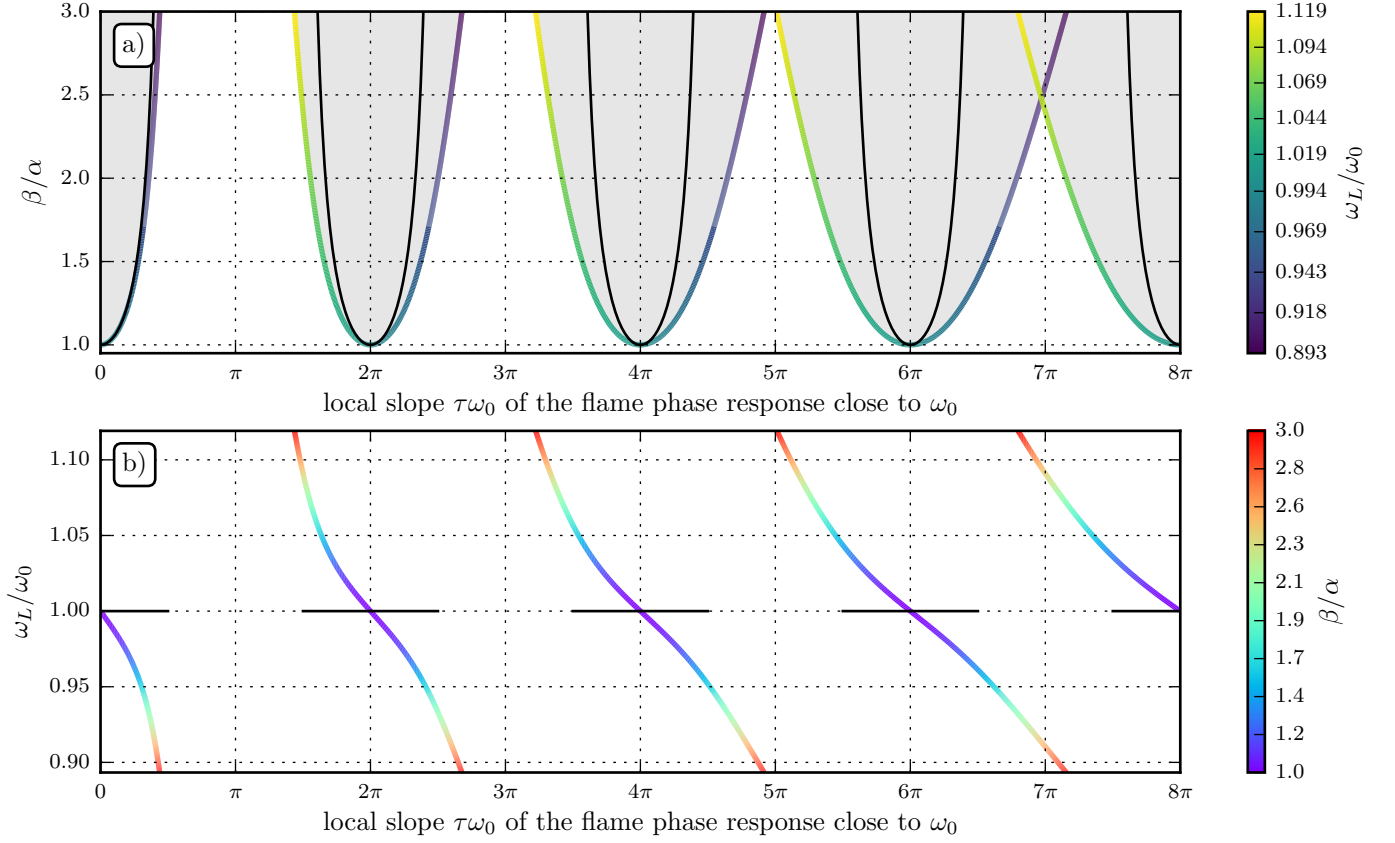
Figure 4: a) boundary of neutral stability as function of the local slope $\tau\omega_0$ of the flame phase response. The coloured line is the ratio of the linear driving β over to the acoustic damping α to make the system neutrally stable. The linearly unstable region is filled in grey. b) The coloured line is the frequency of neutral stability ω_L/ω_0 on the boundary described in a). In both frames the black line is the simpler solution obtained neglecting the part of the heat release rate q not in phase with the pressure p as assumed in Schuermans et al. [19], Noiray et al. [13]

more likely to make the system pulsate because the troughs are broader; *ii)* are more likely to lead to larger frequency shifts from the natural acoustic frequencies $\{\omega_0^k\}$. We advise the reader however to not jump to the hasty conclusion that shorter values of τ lead to fewer pulsations. For example longer convective time delays from the injection point lead to better mixing which reduce in turn the amplitude of equivalence ratio fluctuations at the flame, and longer flames have a larger standard deviation χ in (7). Both factors usually lead to a smaller equivalent gain β in (8).

In the same Figs. 4.a and 4.b we present with black lines the result obtained neglecting the part of heat release rate out of phase with the pressure as assumed in Schuermans et al. [19], Noiray et al. [13], so that one can compare the results with and without assumption. In Fig. 4.a we observe that the black troughs are exactly the same and simply shifted by 2π on the horizontal axis $\tau\omega_0$, so that the error on the boundary of instability increases for larger values of $\tau\omega_0$. A zoom for small values of $\tau\omega_0$ can be found in Figs. 3. As expected, in Fig. 4.b we show how the predicted frequency of oscillation matches ω_0 at all linearly unstable conditions.

As mentioned at the end of §2.3, the plots presented here are for a fixed value of $\alpha/\omega_0 = 0.08$ that was estimated as representative of thermoacoustic systems. We mention that for a fixed value of the ratio β/α, smaller(larger) values of α and

hence β lead to smaller(larger) frequency shifts of ω from ω_0 for a fixed value of $\tau\omega_0$ in Fig. 4.b. Physically, this has the simple interpretation that if the acoustics are little damped and little amplified, the purely acoustic frequency is little affected by them. In Fig. 5 we present the generalization for $\psi \neq 0$ in (8) for 4 different values of the phase ψ. The major and expected change regards a shift of the troughs of ψ on the horizontal axis, and does not affect any of the considerations made on Fig. 4, which is easier to interpret. An interesting conclusion that one can draw from Fig. 5 is that there exist flames that will make the system pulsate regardless of their phase response. For example a flame with $\tau\omega_0 = 7\pi$ and $\beta/\alpha \gtrsim 2.5$ corresponds to a point in Fig.5 that is always unstable regardless of the value of ψ.

4 NONLINEAR ANALYSIS

In this section we apply two nonlinear methods to predict analytically the amplitudes and frequencies of oscillation. As compared to previous work on the topic, the major novelty is in the fact that we explicitly calculate how the instantaneous frequency of oscillation varies as a function of the amplitudes of oscillations, instead of fixing it to a constant value, as presented for example in Fig. 1.b The section is structured so that a reader mostly interested in the results can directly start read-
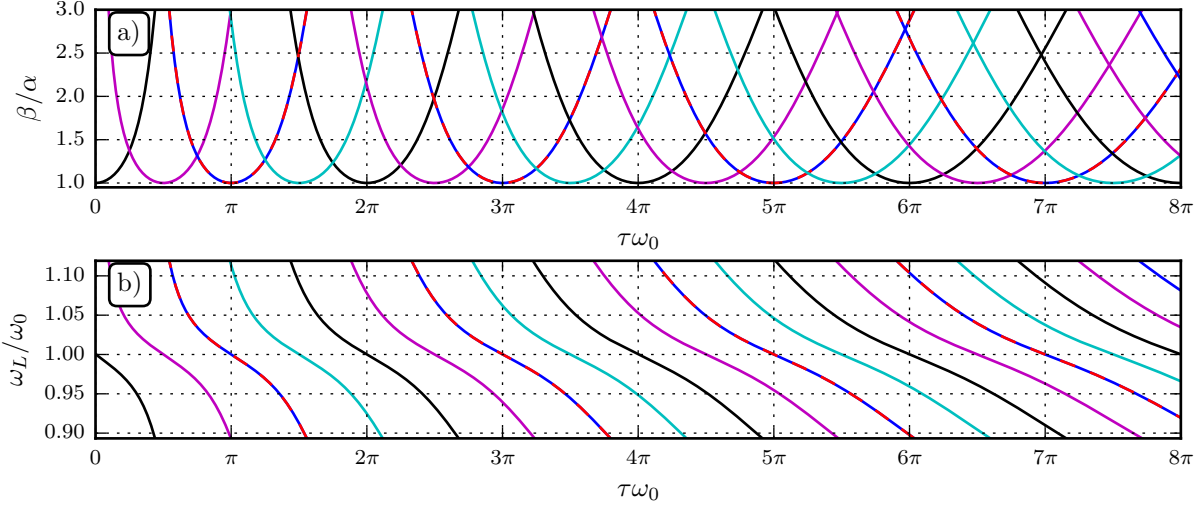
Figure 5: Same as Fig. 4 but without colormaps and for different values of the phase response ψ introduced in (8): black ($\psi = 0$, reference line), magenta ($\psi = \pi/2$), blue/red ($\psi = \pm\pi$), cyan ($\psi = -\pi/2$). The black curves here are the coloured curves of Fig. 4.

ing at §4.5. In §4.1 we apply the method of averaging, and in §4.3 we apply the method of multiple scales, and validate both numerically in §4.4.

4.1 METHOD OF AVERAGING

In this section we apply first order averaging to the model, as defined and discussed in Sanders and Verhulst [18]. We rewrite (10) as a first order system $(x_j, y_j) \equiv (\eta_j, \eta_j')$:

$$x_j'(t) = y_j(t) \tag{25a}$$
$$y_j'(t) = -\omega_0^2 x_j(t) + f_j \tag{25b}$$

where $f_1 = f(y_1(t), y_1(t - \tau), y_2(t - \tau))$ and $f_2 = f(y_2(t), y_2(t - \tau), y_1(t - \tau))$. We introduce the change of variables $(x_j, y_j) \rightarrow (A_j, \varphi_j)$:

$$\begin{cases} 2x_j(t) = A_j(t)e^{i(\omega t + \varphi_j(t))} + \text{c.c.} \\ 2y_j(t) = i\omega A_j(t)e^{i(\omega t + \varphi_j(t))} + \text{c.c.} \end{cases} \tag{26}$$

where c.c. denotes the complex conjugate of the expression to its left. We then substitute (26) into (25), and add (25a) multiplied by $ie^{i(\omega t + \varphi_j)}\omega$ and (25b) multiplied by $-e^{i(\omega t + \varphi_j)}$. We obtain

$$\frac{\omega^2 - \omega_0^2}{2} A_j e^{2i(\omega t + \varphi_j(t))} + \omega \left(\varphi_i'(t) + \frac{\omega}{2} - \frac{\omega_0^2}{2\omega} \right) A_j(t) + i\omega A_j'(t) =$$
$$- e^{i(\omega t + \varphi_j(t))} f_j(t, A_1(t), A_1(t), \ldots) \tag{27}$$

where f depends on the fast time variable t and on the slow variables, which are the amplitudes $A_1(t), A_2(t), A_1(t-\tau), A_2(t-\tau)$ and the phases $\varphi_1(t), \varphi_2(t), \varphi_1(t-\tau), \varphi_2(t-\tau)$. Notice that f is periodic in its direct dependence on t, with period $2\pi/\omega$. We apply first order averaging as discussed by Sanders and Verhulst [18]: we approximate the slow variables as constant in the period of oscillation $2\pi/\omega$ and time-average both sides of (27). The first term on the left hand side has

period π/ω and vanishes out. We are left with:

$$\left(\varphi_i'(t) + \frac{\omega}{2} - \frac{\omega_0^2}{2\omega} \right) A_j(t)\omega + i\omega A_j'(t) \approx \tag{28}$$
$$- \frac{1}{2\pi/\omega} \int_{t-\pi/\omega}^{t+\pi/\omega} e^{i(\omega s + \varphi_j(t))} f_j(s, A_1(t), \ldots) ds$$

In the integral on the right hand side, the delayed slow variables such as $A_1(t - \tau)$ are approximated as $A_1(t)$ since the delay τ is assumed to be of the same order as the period of oscillation, i.e. small compared to the time scale of the slow variables, as discussed by Wahi and Chatterjee [20], Saha et al. [17]. We will relax this assumption later in §5.

We then evaluate the right hand side RHS_j of (28). We take the constant term $e^{i\varphi_j(t)}$ out of the integral, introduce the point $z = e^{i\omega s}$ on the complex unit circle and change the integration variable from s to z, obtaining a closed path integral on the unit circle around the origin:

$$RHS_j = -e^{i\varphi_j(t)} \frac{1}{2\pi i} \oint f_j(z, A_1(t), \ldots) dz \tag{29}$$
$$= -e^{i\varphi_j(t)} \text{Res}_{z=0}[f_j] \tag{30}$$

The term $f_j(z, A_1(t), \ldots)$ is a Laurent polynomial in z, and is then holomorphic everywhere except at $z = 0$, so that in the last passage above we applied the residue theorem. The residue is the coefficient of $1/z$ in the expression of f_j. The right hand side of (28) divided by ω for $j = 1$ evaluates to

$$g(A_1, A_2, \varphi) \equiv \frac{RHS_1}{\omega} = -\frac{e^{i\varphi_1(t)}}{\omega} \text{Res}_{z=0}[f_1] \tag{31a}$$
$$= \frac{1}{2} iA_1 \left(\beta e^{i\tau\omega} - \alpha \right) - \ldots$$
$$\ldots \frac{3}{32} iA_1 \kappa \omega^2 e^{i\tau\omega} \left(A_2^2 e^{2i\varphi} + 3A_1^2 + 2A_2^2 \right)$$

where φ is the difference between the phases of the first and second oscillator, $\varphi \equiv \varphi_1 - \varphi_2$, and the expression for g_2 is

8

obtained similarly. In particular one finds

$$\frac{RHS_2}{\omega} = g(A_2, A_1, -\varphi) \tag{31b}$$

We divide both sides of (28) by ω, substitute (31), and obtain the equations for the time evolution of the slow variables of the two oscillators:

$$\left(\varphi_1'(t) + \frac{\omega}{2} - \frac{\omega_0^2}{2\omega}\right) A_1(t) + iA_1'(t) = g(A_1, A_2, +\varphi) \tag{32a}$$

$$\left(\varphi_2'(t) + \frac{\omega}{2} - \frac{\omega_0^2}{2\omega}\right) A_2(t) + iA_2'(t) = g(A_2, A_1, -\varphi) \tag{32b}$$

with $\varphi \equiv \varphi_1 - \varphi_2$. This dynamical system is in terms of the variables $\{A_1, A_2, \varphi_1, \varphi_2\}$ and can present solutions where both phases φ_1 and φ_2, in the limit $t \to \infty$, present a common oblique asymptote, i.e. the two oscillators undergo the same shift of their oscillation frequency. However, these solutions are not fixed points of (32) since $\varphi_j'(t) \neq 0$. These solutions are however fixed points of an equivalent system, in terms of the variables $\boldsymbol{x} = \{A_1, A_2, \varphi, \varphi_{avg} \equiv (\varphi_1 + \varphi_2)/2\}$:

$$A_1' = \frac{A_1}{2}(\beta\cos(\tau\omega) - \alpha) - \frac{3}{32}A_1\kappa\omega^2(A_2^2\cos(\tau\omega + 2\varphi) + \quad \ldots$$
$$\ldots \quad 3A_1^2\cos(\tau\omega) + 2A_2^2\cos(\tau\omega)) \tag{33a}$$

$$A_2' = \frac{A_2}{2}(\beta\cos(\tau\omega) - \alpha) - \frac{3}{32}A_2\kappa\omega^2(A_1^2\cos(2\varphi - \tau\omega) + \quad \ldots$$
$$\ldots \quad 2A_1^2\cos(\tau\omega) + 3A_2^2\cos(\tau\omega)) \tag{33b}$$

$$\varphi' = \frac{3}{16}\kappa\omega^2\sin(\varphi)\left(A_1^2\cos(\varphi - \tau\omega) + A_2^2\cos(\varphi + \tau\omega)\right) \tag{33c}$$

$$\varphi_{avg}' + \frac{\omega}{2} = \frac{\omega_0^2}{2\omega} - \frac{1}{2}\beta\sin(\tau\omega) + \frac{3}{64}\kappa\omega^2(A_2^2\sin(\tau\omega + 2\varphi) - \quad \ldots$$
$$\ldots \quad A_1^2\sin(2\varphi - \tau\omega) + 5(A_1^2 + A_2^2)\sin(\tau\omega)) \tag{33d}$$

In (33), the first three equations describe the amplitudes and the synchronization of the two oscillators: the fixed points of these three equations in the three variables $\{A_1, A_2, \varphi\}$, which depend parametrically in ω, are the synchronized solutions of the system. The role of the last equation (33d) will be commented in the next section §4.2.

For a fixed value of ω there are only two stable solutions among the fixed points of the system of equations (33a),(33b) and (33c). These stable solutions are spinning waves and have amplitudes:

$$\begin{cases} A_1 = A_2 = \frac{2}{\sqrt{3}\omega}\sqrt{\frac{\beta - \alpha\sec(\tau\omega)}{\kappa}} \\ \varphi = \pm\pi/2 \end{cases} \tag{34}$$

4.2 THE CHOICE OF ω

We recall that ω defines the period $2\pi/\omega$ over which we carry out the time averaging, so that we should always choose ω to match the instantaneous frequency of oscillation of the oscillator in order to average exactly over one period of oscillation. When applying the method of averaging, one often assumes

that the frequency of oscillation ω is close to the natural frequency of oscillation ω_0 of the unperturbed oscillator, and approximate $\omega \approx \omega_0$. This assumption is often carried out earlier in the analysis, by fixing $\omega = \omega_0$ in (26). We have however observed in §3 that the frequency of oscillation ω_L of the neutrally stable, linearized system departs from ω_0, and is most noticeably dependent on τ, as in Fig. 4.b.

We can improve the choice of ω from ω_0 by using equation (33d), and choosing ω such that the mean average phase φ_{avg} is a fixed point of the system too. This also means that the frequency of averaging ω of the system matches the instantaneous frequency of the two oscillators, since we have that

$$\omega_{avg}^{inst} = \frac{\partial}{\partial t}\frac{(\omega t + \varphi_1(t)) + (\omega t + \varphi_2(t))}{2} = \omega + \varphi_{avg}'(t) \tag{35}$$

This leads to an equation for ω:

$$\omega^2 = \omega_0^2 - \beta\omega\sin(\tau\omega) + \frac{3}{32}\kappa\omega^3(A_2^2\sin(\tau\omega + 2\varphi) - \quad \ldots$$
$$\ldots \quad A_1^2\sin(2\varphi - \tau\omega) + 5(A_1^2 + A_2^2)\sin(\tau\omega)) \tag{36}$$

In the linear regime $A_i \to 0$, and from (36) we recover the linear dispersion relation (15b), with the difference that this time it is not calculated on the boundary of instability, i.e. equation (15a) does not hold.

In the general nonlinear regime before saturation, the frequency of oscillation shifts from this value and it is dependent on the two amplitudes A_1 and A_2 and also on φ as described by (36). We numerically integrate in time the first three equations (33), and at each timestep calculate the instantaneous frequency ω which satisfies (36). An example of a simulation is reported in Fig. 1, where A_1, A_2 and φ are reported as dotted lines.

In the nonlinear regime but at the converged limit cycle solution, we can calculate the frequency ω_{LC} of oscillation by substituting (34) into (36), and obtain:

$$h(\tau, \omega_{LC}) \equiv \omega_{LC}^2 - \omega_0^2 + \alpha\omega_{LC}\tan(\omega_{LC}\tau) = 0 \tag{37}$$

We observe that this matches equation (20) for ω_L, which is the frequency of the neutrally stable system obtained by reducing the linear driving coefficient β until neutral stability is reached[4]. In other words, the frequency at the limit cycle matches the frequency of the linear system obtained by suitably reducing the flame response to make it neutrally stable.

To numerically integrate in time the system of equations (33), at each time step we numerically solve equation (36) for ω, and then calculate the right hand sides of (33) and proceed at the next time step.

We now show an example of the predictions of equation (35) in a time domain simulation. In Fig. 1.b we compare the instantaneous frequency ω as extracted from the original oscillators and the solution ω^{AVG} of (36) calculated as a function of the instantaneous amplitudes A_j. We have overall very good agreement, while we observe some small error in the fully linear and fully nonlinear regime.

---

[4]indeed, β is reduced when it is calculated in (19)

In the fully linear regime at the left of Fig. 1.b the error between the frequency ω^{AVG} and the frequency of the linearized system is due to an inherent limitation of the method of averaging, which assumes that η_j and $\partial\eta_j/\partial t$ are exactly out of phase. This is exact at the limit cycle if one neglects higher order harmonics, while the error made is largest where the growth rates are largest, which in this case is at the onset of oscillation. This error is however marginal and smaller than 0.02% in this time simulation. In the fully nonlinear regime at the right of Fig. 1.b the error between the frequency ω^{AVG} and the predicted frequency of oscillation ω_L is due to the fact that we are neglecting the contribution of higher order harmonics that in this case makes the amplitudes A_j just 1.5% smaller than the prediction A^{AVG}. This in turn affects the amplitudes in (36), leading to an error however smaller than 0.02%.

We add a final note on the formal correctness of this derivation where the frequency of oscillation ω depends on time. The time-derivatives of $\{\eta_j, \eta_j'\}$ are $O(1)$ quantities i.e. are governed by time t. The method of averaging assumes that the slowly varying amplitudes and phases are $O(\varepsilon)$ quantities, i.e. are governed by time $T \equiv \varepsilon t$. In equation (27) we keep the terms that are $O(\varepsilon)$ i.e. we keep the time derivatives of the slow flow variables. In the passage to obtain (27), and more clearly in the passage in (35), we are implicitly assuming that the time derivative of ω can be neglected, i.e. we assume that $\partial\omega/\partial t$ is a term that scales with $O(\varepsilon^2)$ and neglect it. We present evidence that this approximation is reasonable in Fig. §1.b, where we observe that ω^{AVG} is rather close to the reconstructed value of ω especially in the regions where $\partial\omega/\partial t \neq 0$.

4.3 THE METHOD OF MULTIPLE SCALES

We apply the method of multiple scales. Because of the required brevity of this publication, we do not report the derivation that can be found in Ghirardo [7]. One obtains the set of equations:

$$A_1' = A_1 \frac{L - \kappa N_A(A_1^2, A_2^2, +\varphi)}{D} \tag{38a}$$

$$A_2' = A_2 \frac{L - \kappa N_A(A_2^2, A_1^2, -\varphi)}{D} \tag{38b}$$

$$\varphi' = \kappa \frac{N_\varphi(A_1^2, A_2^2, \varphi)}{D} \tag{38c}$$

$$\varphi_{avg}' = \frac{N_{\varphi_{avg}}(A_1^2, A_2^2, \varphi)}{2D} \tag{38d}$$

where the expressions of $L, N_A, N_\varphi, N_{\varphi_{avg}}$ and D are reported in appendix §A, and the method predicts the instantaneous frequency of oscillation as $\omega^{MMS}(t) = \omega_L + \frac{d\varphi_{avg}}{dt}$. In the first two equations, L/D is a linear growth coefficient and the term N_A/D is responsible for the nonlinear saturation of the amplitudes. The third equation governs the synchronization of the two oscillators, and depends only on nonlinear terms, since it is proportional to κ. The right hand side of (38d) is the frequency shift of the two oscillators, which depends on the amplitude of oscillation.

There are only two stable solutions among the fixed points of the system of equations (38a),(38b) and (38c) and they match exactly the solutions (34) of the method of averaging.

The mean frequency of oscillation of the limit cycle is ω_L, because once we substitute (34) into (38d) we find that the numerator on the right hand side evaluates to zero. This means that the method of multiple scales predicts that the frequency of oscillation at the limit cycle matches ω_L, matching the prediction of the method of averaging.

For completeness, we present the instantaneous frequency of oscillation using the method of multiple scales as $\omega^{MMS}(t)$ in Fig.1.b. The performance of this estimate is overall similar to the method of averaging, slightly better in the linear regime at small amplitudes.

4.4 ACCURACY OF THE NONLINEAR SOLUTION

We tested the quality of these analytical solutions for a series of numerical simulations using the solver PYDELAY [6]. In particular we fix $\alpha = 0.08$ and run simulations of (10) on a fine grid with 153 values of β/α equispaced between 0 and 3 and 337 values of $\tau\omega_0$ equispaced between 0 and 8, for a total of 51561 simulations. We started the numerical integration at $t = 0$, with a history function defined for $t \in [0, -\tau]$ that is oscillatory. We then extract the amplitude and the frequency of the solutions once the numerical code has converged to a limit cycle. We report the amplitude in Fig. 6.a, and the frequency in Fig. 6.b. The agreement is overall very good, except a small discrepancy for small values of β/α, where the contour line of the numerical solution at $A = 0.051$ is slightly jagged and slightly underpredicts the analytical solution in a few regions. This is due to the fact that we extracted the amplitudes from the numerical solutions too early in time, before the system had fully converged to the limit cycle. This is corroborated by the fact that for a constant α, smaller values of β/α make the system more weakly nonlinear, leading to longer time-scales for the evolution of the slow flow variables. On the horizontal line $\beta/\alpha = 3$ at the border of the investigated parameter space, where the system is more strongly nonlinear, the error between the predicted and measured amplitude was found to be smaller than 2.2%. On the same line, the error in the prediction of the frequency of oscillation was smaller than 0.08%.

4.5 DISCUSSION

Using the method of averaging and the method of multiple scales we have obtained two sets of equations, respectively (33) and (38). Despite the fact that the two sets of equations differ, they share the same limit cycle solution, oscillating at the frequency ω_L of the neutrally stable system[5], and at the amplitude described by (34). As discussed in §4.4, the analytical solutions were validated against numerical simulations with excellent agreement, confirming that they characterize correctly the limit cycle solution. We present in Fig. 6 the amplitudes and frequencies of oscillation of the limit-cycle solution. As expected, in Fig. 6.a the amplitude grows from a value of 0 on the boundary of neutral stability as the ratio β/α increases along vertical lines of constant $\tau\omega_0$. Importantly, the smooth amplitude contour of the system in the nonlinear regime confirms that all the practical considerations discussed

---
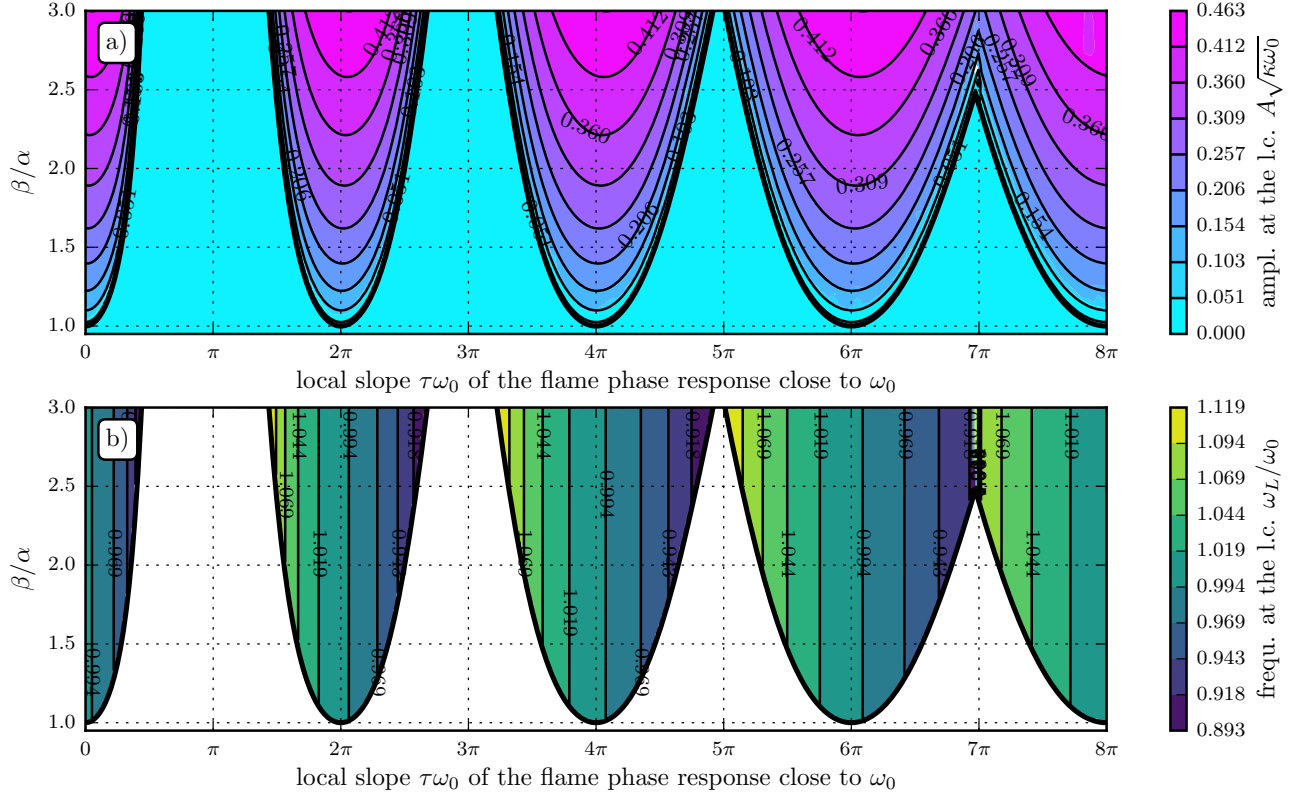
[5]defined as the solution of (15b)

Figure 6: Nonlinear analysis. a) Comparison of the saturated amplitude and frequency at the limit cycle (l.c.) extracted from the numerical integration of the original system of delayed coupled oscillators described by equations (10) (in colour) and of the analytical solution (black lines). a) Amplitude of oscillation $A\sqrt{\kappa\omega_0}$. b) Frequency of oscillation ω/ω_0. In both a) and b) the black lines were chosen to be at the same levels as the colour contour boundaries. The two coincide almost exactly showing that the analytical solution matches the results of the numerical integration of the original system.

in §3.2 hold validity in the nonlinear regime. We observe in 6.b that along vertical lines the frequency of oscillation at the limit cycle is constant, i.e. is independent of β/α. This means that systems with different values of β start with a different, linear frequency of oscillation as in Fig. 1.b, but they all converge to the same frequency of oscillation ω_L. This happens for this specific case, because the chosen nonlinearity in (9) has a phase response that does not depend on amplitude. Both methods predict the evolution of the frequency of oscillation with time, as exemplified in Fig. 1.b. In the general case, sources (flames) and sinks (dampers) have a phase response that depends on the amplitude, leading to larger frequency shifts from the linear to the nonlinear regime. It is especially in these situations that one should take into account in the time domain the dependence of the frequency of oscillation on the amplitudes, as done here in (36).

5 LINEAR GROWTH RATE ESTIMATION

In this section we show how the system of equations assumed by Noiray [12] with a zero delay τ, resembles in a certain mathematical sense the original system of equations with a non-zero delay τ. If this is the case, then one can safely use the methods discussed in [12] for linear growth rate estimation. We leave open the question of the identification of the delay τ and the case of azimuthal instabilities and focus on

a thermoacoustic system with a single mode. When carrying out the projection of the equations (1) on a single mode η_1 and assuming the flame compact in space, one obtains

$$\eta_1''(t)+\omega_0^2\eta_1(t) = f(\eta_1'(t),\eta_1'(t-\tau)),$$
$$\text{with} \quad f(a,a_\tau) = a_\tau(\beta - \kappa a_\tau^2) - \alpha a \quad (39a)$$

The averaged equations for this system are obtained similarly and are:

$$A_1' = A_{1,\tau}\left[\nu - \mu A_{1,\tau}^2\right] \quad (39b)$$

$$\varphi_1' = -\frac{\beta}{2}\sin(\tau\omega) + \mu A_{1,\tau}^2 + \frac{\omega 0^2}{2\omega} - \frac{\omega}{2} \quad (39c)$$

where we introduce

$$\begin{cases} \nu = (\beta\cos(\tau\omega) - \alpha)/2 \\ \mu = 3\kappa\cos(\tau\omega)\omega^2/8 \end{cases} \quad (40)$$

Notice how the amplitude A_1 on the right hand side of (39b) is delayed, i.e. $A_{1,\tau}(t) = A_1(t - \tau)$. In other words, we are not here assuming as done just after (28) that the delay τ is small compared to the time scale of A_1', because this section focuses in detail on the growth rate of A_1[6]. Remarkably, the limit cycle solution of (39) has the same amplitude A and the

---

[6]Notice that this does not affect any of the results of §4.1

11

same frequency ω_L of the solution of the problem with two modes[7], meaning that the nonlinear results of Fig. 6.a apply also to a single mode:

$$A = \sqrt{\frac{\nu}{\mu}} = \frac{2}{\sqrt{3}\omega_L}\sqrt{\frac{\beta - \alpha\sec(\tau\omega_L)}{\kappa}},$$

$$\text{with } \omega_L \text{ solution of (20)} \qquad (41)$$

We observe that the frequency of oscillation $\omega(t)$ is close to ω_L and in the following assume that $\omega(t) = \omega_L \; \forall t$ in (39b) and discard the study of the equation for φ_1.

Noiray [12] identifies a system of equations like (39a) but with $\tau_{(E)}$ set to zero:

$$\eta_1''(t) + \omega_{0(E)}^2\eta_1(t) = f(\eta_1'(t), \eta_1'(t-\tau)),$$

$$\text{with} \quad f(a) \equiv a(\beta_{(E)} - \kappa_{(E)}a^2) - \alpha a \qquad (42a)$$

with the respective slow flow equation:

$$A_1' = A_1\left[\nu_{(E)} - \mu_{(E)}A_1^2\right] \qquad (42b)$$

We then want to understand if there exists a set of coefficients $\{\nu_{(E)}, \mu_{(E)}, \omega_{0(E)}\}$ such that the dynamics of the equivalent (hence the subscript $_{(E)}$) system (42b) matches the dynamics of the original system (39b), so that the system identification would identify it. We first observe that the frequency of oscillation of (42a) is well approximated by $\omega_{0(E)}$, so that it has to be $\omega_{0(E)} = \omega_L$. We then observe that in principle the dynamics of (39b) and (42b) cannot match because the first is of delayed differential type, while the second is of ordinary differential type. We can however approximate the Taylor expansion of the delayed term to the first order in τ:

$$A_{1,\tau} = A_1(t-\tau) \approx A_1(t) - \tau A_1'(t) + \mathcal{O}(\tau^2) \qquad (43)$$

By substituting (43) into (39b) and after some manipulation we obtain:

$$A_1'(1 + \nu\tau - 3\mu\tau A_1^2) = \nu A_1 - \mu A_1^3 \qquad (44)$$

Despite the fact that (44) does not have the same structure as (42b) in the nonlinear regime, one can expand in Maclaurin series the expression of A_1' in powers of A_1, truncate it to the third order, and match suitably the coefficients $\{\nu_{(E)}, \mu_{(E)}\}$. In the linear regime the two systems are equivalent:

$$\sigma^{(E)} = \nu_{(E)} \approx \frac{\nu}{1 + \tau\nu} \qquad (45)$$

where $\sigma^{(E)}$ is the growth rate of (42a).

A similar argument can be applied with the method of multiple scales. In the linear regime the two modes A_1 and A_2 are decoupled in (38) and the linear coefficient matches the case of one thermoacoustic mode only. In this case the system is already of ordinary differential type, and one expects that

$$\sigma^{(E)} = \nu_{(E)} \approx \frac{L}{D} \qquad (46)$$

We find good qualitative agreement in Fig. 7 between the exact growth rate of (39a) in blue, the growth rate (45) in red,

and the growth rate (46) in green, with the discrepancies to be attributed to the not perfect accuracy of the two nonlinear methods. As a comment, we observe in Fig. 7 a reduction as a function of $\tau\omega_0$ of all three growth rates. This effect of the delay τ can be observed in eq. (45) and is additional to the direct effect of the phase $\tau\omega$ between q and p accounted for in the $\cos(\tau\omega)$ term in the definition (40) of ν. To conclude, we observe that equations (42) used by Noiray [12], with suitable coefficients $\{\nu_{(E)}, \mu_{(E)}\}$, match either the third order Maclaurin expansion of the equations (44) of the truncated method of averaging, or the equations of the method of multiple scales for one mode, under certain mathematical approximations. Then it follows that the system identification method [12] applied to timeseries of the original system (39) with delay should produce good growth rate estimates of the original system, within the limits of these approximations. The mismatch in Fig. 7 shows that some of these approximations play a limited role. This approximate equivalence between the models with and without delay is in line with past experience (Bothien et al. [2]) with growth rate predictions on a model with a time delay, but requires further numerical evidence.

6 CONCLUSIONS

We discuss the effect of the local nondimensional slope $\tau\omega_0$ of the flame phase response in the vicinity of the frequency ω_0 of the considered acoustic mode of the system, both in the linear and nonlinear regime. The results apply both to systems with either only one mode oscillating, or two degenerate azimuthal modes oscillating. In §2 we carry out a brief derivation of the problem, introduce τ as the local flame phase response slope, and compare this formulation with the literature.

In §3 we provide new insights regarding the stability of thermoacoustic systems. We show for example that: *1)* flames with a steep phase response are more likely to trigger pulsations and to lead to larger frequency shifts from ω_0; *2)* a flame responding in anti-phase with the pressure p at the frequency ω_0 can still make the system unstable; *3)* a flame can destabilize an acoustic mode regardless of its phase response at ω_0.

In §4 we adjust the method of averaging to account for a frequency of oscillation ω that does not match the natural frequency of oscillation ω_0 of the system. This leads to the derivation of an equation that describes the time evolution of the instantaneous frequency of oscillation $\omega(t)$ as a function of the amplitudes of oscillation of the two modes, which will prove especially useful in situations where a part of the system, e.g. a flame or a damper, has a phase response that depends on the amplitude. Both nonlinear methods lead to excellent results in the typical range of the parameters that characterize thermoacoustic oscillations. The nonlinear results of Fig. 6 extend the validity of the considerations of §3 in the nonlinear regime.

In §5 we present a conjecture suggesting that one may neglect the part of heat release rate q in quadrature with the pressure p when estimating the linear growth of a time series, with this line of reasoning. Despite the fact that one cannot assume that the nonlinear frequency of oscillation ω matches the natural acoustic frequency of oscillation ω_0, one can instead

---

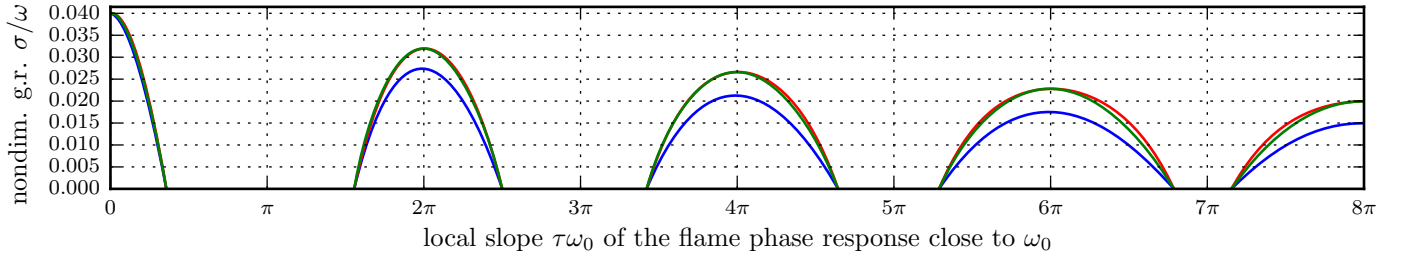[7]solutions for the two modes were presented in (34)

Figure 7: Linear growth rates (g.r.) of: the original equations of the system (39) with delay (blue), the truncated equations of the method of averaging (red), the equations of the method of multiple scales (green). These results are for $\beta/\alpha = 2, \alpha/\omega = 0.08$.

average over the nonlinear frequency of oscillation ω_L, and reconstruct the linear growth rate of an equivalent thermoacoustic system where the natural acoustic frequency of oscillation is ω_L, and the part of heat release rate q in quadrature with the pressure p is neglected. The slowly varying equations governing this equivalent system are shown to match, within the boundaries of a set of mathematical approximations, the slowly varying equations of the original system, hence suggesting that the identified growth rate using the equations of the equivalent system should be close to the exact growth rate of the original system, as previous experience of Bothien et al. [2] suggested. A quantitative discussion of this conjecture will require further numerical validation.

Nomenclature

′   the prime denotes time derivative of the preceding quantity

ˆ   the hat denotes the Fourier transform of the underlying quantity

α equivalent acoustic damping coefficient, appearing in (1b)

β linear flame response gain as function of p, as in $|q| \propto \beta|p|$

η'_j amplitudes of the acous. pres. of the 2 azim. modes as in (2), for $j = 1, 2$

κ nonlinear saturation coefficient, appearing in (9)

ω angular frequency

ω_0 acoustic frequency of oscillation when the flame and the damping are virtually shut off

ω_L frequency of the system if the flame response gain β is virtually decreased until the system is neutrally stable, i.e. $\sigma = 0$. We prove that ω_L is also the frequency of the limit-cycle solution for this studied case.

ω_{LC} frequency of oscillation at the limit cycle

ψ phase response at $\omega = 0$ of the fit (8) around ω_0 of the flame response

σ growth rate

τ equivalent time delay of the transfer function $\hat{q}/\hat{p}$ as introduced in (8), e.g. local slope of of the phase response of such transfer function at frequencies close to ω_0.

θ azimuthal coordinate, $\theta \in [0, 2\pi)$

a h

A_j Slowly varying amplitudes of oscillations, introduced in (26)

n azimuthal order of the mode, e.g. $n = 3$ refers to the third azimuthal

$n\eta_j$ amplitudes of the acous. vel. of the 2 azim. modes as in (2), for $j = 1, 2$

p acoustic pressure, suitably nondimensionalized

q fluctuating heat release rate, suitably nondimensionalized, often called flame response

u acoustic velocity in the azim. direction, suitably nondimensionalized

u_{ax} acoustic velocity in the axial direction, typically long the axis of the burner, suitably nondimensionalized

References

[1] Bonciolini, G., Boujo, E., and Noiray, N. (2016). Effects of turbulence-induced colored noise on thermoacoustic instabilities in combustion chambers. In *International Symposium: Thermoacoustic Instabilities in Gas Turbines and Rocket Engines*, May 30 - June 02, 2016 Munich (DE).

[2] Bothien, M. R., Noiray, N., and Schuermans, B. (2015). Analysis of Azimuthal Thermo-acoustic Modes in Annular Gas Turbine Combustion Chambers. *Journal of Engineering for Gas Turbines and Power*, 137(6):061505.

[3] Boudy, F., Durox, D., Schuller, T., Jomaas, G., and Candel, S. (2011). Describing Function Analysis of Limit Cycles in a Multiple Flame Combustor. *Journal of Engineering for Gas Turbines and Power*, 133(6):061502.

[4] Candel, S., Durox, D., Schuller, T., Bourgouin, J.-F., and Moeck, J. P. (2014). Dynamics of Swirling Flames. *Annual Review of Fluid Mechanics*, 46(1):147–173.

[5] Ducruix, S., Schuller, T., Durox, D., and Candel, S. (2003). Combustion Dynamics and Instabilities: Elementary Coupling and Driving Mechanisms. *Journal of Propulsion and Power*, 19(5):722–734.

[6] Flunkert, V. and Schoell, E. (2009). Pydelay - a python tool for solving delay differential equations. *ArXiv*.

[7] Ghirardo, G. (2016). *Nonlinear analysis of thermoacoustic modes in axisymmetric annular combustors*. PhD thesis, University of Cambridge.

[8] Ghirardo, G., Ćosić, B., Juniper, M. P., and Moeck, J. P. (2015). State-space realization of a describing function. *Nonlinear Dynamics*, 82(1-2):9–28.

[9] Ghirardo, G. and Juniper, M. P. (2013). Azimuthal instabilities in annular combustors: standing and spinning modes. *Proceedings of the Royal Society A: Mathematical, Physical and Engineering Sciences*, 469(2157):20130232.

[10] Ghirardo, G., Juniper, M. P., and Moeck, J. P. (2016). Weakly nonlinear analysis of thermoacoustic Instabilities in annular combustors. *Journal of Fluid Mechanics*, 805:52–87.

[11] Lieuwen, T. (2003). Modeling Premixed Combustion-Acoustic Wave Interactions: A Review. *Journal of Propulsion and Power*, 19(5):765–781.

[12] Noiray, N. (2016). Linear growth rate estimation from dynamics and statistics of acoustic signal envelope in turbulent combustors. *Proceedings of the ASME TurboExpo 2016 paper no. GT2016-58169*, pages 1–11.

[13] Noiray, N., Bothien, M. R., and Schuermans, B. (2011). Investigation of azimuthal staging concepts in annular gas turbines. *Combustion Theory and Modelling*, 15(5):585–606.

[14] Noiray, N., Durox, D., Schuller, T., and Candel, S. (2008). A unified framework for nonlinear combustion instability analysis based on the flame describing function. *Journal of Fluid Mechanics*, 615(2008):139–167.

[15] Noiray, N. and Schuermans, B. (2013). Deterministic quantities characterizing noise driven Hopf bifurcations in gas turbine combustors. *International Journal of Non-Linear Mechanics*, 50:152–163.

[16] RAYLEIGH (1878). The Explanation of Certain Acoustical Phenomena. *Nature*, 18(455):319–321.

[17] Saha, A., Bhattacharya, B., and Wahi, P. (2010). A comparative study on the control of friction-driven oscillations by time-delayed feedback. *Nonlinear Dynamics*, 60(1-2):15–37.

[18] Sanders, J. A. and Verhulst, F. (2007). *Averaging Methods in Nonlinear Dynamical Systems*, volume 59 of *Applied Mathematical Sciences*. Springer, 2nd edition.

[19] Schuermans, B., Paschereit, C. O., and Monkewitz, P. (2006). Non-Linear Combustion Instabilities in Annular Gas-Turbine Combustors. In *44th AIAA Aerospace Sciences Meeting and Exhibit. Paper no. AIAA-2006-0549*, Reston, Virginia. American Institute of Aeronautics and Astronautics.

[20] Wahi, P. and Chatterjee, A. (2004). Averaging Oscillations with Small Fractional Damping and delayed terms. *Nonlinear dynamics*, 38:3–22.

A SLOW FLOW EQUATIONS

We report in (47) the expressions introduced in (38):

$$
\begin{aligned}
D = {}& 16\Big(\alpha^2 + \big(4(\alpha\tau + 1)\omega_L^2 - \alpha^2\big)\cos\left(2\tau\omega_L\right) + 2(\alpha\tau(\alpha\tau + 2) + 2)\omega_L^2 + 2\alpha(\alpha\tau + 2)\omega_L\sin\left(2\tau\omega_L\right)\Big) \\
L = {}& -16\omega_L\left(\alpha - \beta\cos\left(\tau\omega_L\right)\right)\left(\alpha\sin\left(2\tau\omega_L\right) + 2\omega_L\left(\alpha\tau + \cos\left(2\tau\omega_L\right) + 1\right)\right)
\end{aligned}
\tag{47a}
$$

$$
\begin{aligned}
N_A(A_1^2, A_2^2, \varphi) = {}& 3\omega_L^3\Big(2\omega_L\left(A_2^2\cos(2\varphi) + 3A_1^2 + 2A_2^2\right)\cos\left(\tau\omega_L\right)\left(\alpha\tau + \cos\left(2\tau\omega_L\right) + 1\right) \\
& + \sin\left(2\tau\omega_L\right)\left(\cos\left(\tau\omega_L\right)\left(\alpha A_2^2\cos(2\varphi) + 3\alpha A_1^2 + 2\alpha A_2^2 - 2A_2^2\omega_L\sin(2\varphi)\right)\right. \\
& \left. - \alpha A_2^2\sin(2\varphi)\sin\left(\tau\omega_L\right)\right)\Big)
\end{aligned}
\tag{47b}
$$

$$
\begin{aligned}
N_\varphi(A_1^2, A_2^2, \varphi) = {}& 6\omega_L^3\sin(\varphi)\cos\left(\tau\omega_L\right)\Big(2\left(A_1^2 - A_2^2\right)\sin(\varphi)\sin\left(\tau\omega_L\right)\left(\alpha\sin\left(\tau\omega_L\right) + 2\omega_L\cos\left(\tau\omega_L\right)\right) \\
& + \left(A_1^2 + A_2^2\right)\cos(\varphi)\left(\alpha\sin\left(2\tau\omega_L\right) + 2\omega_L\left(\alpha\tau + \cos\left(2\tau\omega_L\right) + 1\right)\right)\Big)
\end{aligned}
\tag{47c}
$$

$$
\begin{aligned}
N_{\varphi_{avg}}(A_1^2, A_2^2, \varphi) = {}& \omega_L\Big(\sin\left(2\tau\omega_L\right)\left(\alpha\sin\left(\tau\omega_L\right) + 2\omega_L\cos\left(\tau\omega_L\right)\right)\left(15\left(A_1^2 + A_2^2\right)\kappa\omega_L^2 - 32\beta + 32\alpha\sec\left(\tau\omega_L\right)\right) \\
& + 3\left(A_1^2 + A_2^2\right)\kappa\omega_L^2\cos(2\varphi)\sin\left(2\tau\omega_L\right)\left(\alpha\sin\left(\tau\omega_L\right) + 2\omega_L\cos\left(\tau\omega_L\right)\right) \\
& - 3\left(A_1^2 - A_2^2\right)\kappa\omega_L^2\sin(2\varphi)\cos\left(\tau\omega_L\right)\left(\alpha\sin\left(\tau\omega_L\right) + 2\omega_L\left(\alpha\tau + \cos\left(2\tau\omega_L\right) + 1\right)\right)\Big)
\end{aligned}
\tag{47d}
$$